Available online at www.sciencedirect.com
ScienceDirect
Journal of Solid State Chemistry 180 (2007) 1209–1217
JOURNAL OF SOLID STATE CHEMISTRY
www.elsevier.com/locate/jssc

Structural characterization, magnetic behavior and high-resolution EELS study of new perovskites $Sr_2Ru_{2-x}Co_xO_{6-\delta}$ ($0.5 \leqslant x \leqslant 1.5$)

A.D. Lozano-Gorrín[a,b,c,*], J.E. Greedan[a,b], P. Núñez[c], C. González-Silgo[d], G.A. Botton[a], G. Radtke[a]

[a]*Brockhouse Institute for Materials Research, McMaster University, Hamilton, Ont., Canada L8S 4M1*
[b]*Department of Chemistry, McMaster University, 1280 Main Street W., Hamilton, Ont., Canada L8S 4M1*
[c]*Departamento de Química Inorgánica, Universidad de La Laguna, 38206-La Laguna, Tenerife, Spain*
[d]*Departamento de Física Fundamental II, Universidad de La Laguna, 38200-La Laguna, Tenerife, Spain*

Received 13 November 2006; received in revised form 10 January 2007; accepted 14 January 2007
Available online 1 February 2007

Abstract

New oxides of general formula $Sr_2Ru_{2-x}Co_xO_{6-\delta}$ ($0.5 \leqslant x \leqslant 1.5$) have been synthesized as polycrystalline materials and characterized structurally by X-ray diffraction. For $0.5 \leqslant x < 0.67$ the orthorhombic, *Pnma*, perovskite structure of the end member, $SrRuO_3$, is found. At $x = 0.67$ a phase separation into an Ru-rich *Pnma* phase and a Co-rich $I2/c$ phase occurs. The $I2/c$ form is also found for $x = 1.0$ but another orthorhombic phase, *Imma*, obtains for $x = 1.33$ and 1.5. Reductive weight losses indicate negligible oxygen non-stoichiometry, i.e., $\delta \sim 0$, for all compositions even those rich in Co. High-resolution electron energy loss spectroscopy (EELS) indicates that cobalt is high-spin Co^{3+} or high-spin Co^{4+} for all x. Appropriate combinations of Ru^{4+}, Ru^{5+}, HS Co^{3+} and HS Co^{4+} are proposed for each x which are consistent with the observed Ru(Co)–O distances. Significant amounts of Co^{4+} must be present for large x values to explain the short observed distances. Broad maxima in the d.c. susceptibilities are found between 78 and 97 K with increasing x, along with zero-field-cooled (ZFC) and field-cooled (FC) divergences suggesting glassy magnetic freezing. A feature near 155 K for all samples indicates a residual amount of ferromagnetic $SrRuO_3$ not detected by X-ray diffraction.

Keywords: Ru–Co perovskites; Solid solution; Miscibility gap; X-ray powder diffraction; Glassy magnetism; Cobalt *L*-edge; Electron energy loss spectroscopy

1. Introduction

Many transition metal oxides show the very versatile perovskite structure. The rich variety of physical properties such as high-temperature superconductivity and colossal magnetoresistence observed in these compounds makes them very attractive from both fundamental and applied perspectives. The structural and electronic properties of perovskite-related materials having the general formulae $A_2BRu^{5+}O_6$ and $AA'BRu^{5+}O_6$ (where A and A' are early lanthanides or alkaline-earth metals and B is a transition metal or one of the smaller lanthanides) have been extensively investigated by a number of research groups [1–7]. These materials crystallize in a wide variety of symmetries depending on factors such as the Goldschmidt tolerance factor and the degree of site ordering between the *B*-site ions. Anderson et al have constructed a phase diagram in which the criteria for *B*-site order are identified [8]. In general, if the radius difference between the *B*-site ions exceeds 0.2 Å and the difference formal charge $\geqslant 2$ *B*-site ordering will occur. Otherwise a random distribution is expected. When the Goldschmidt factor is less than 1, a number of distortions from the ideal $Pm3m$ symmetry are found. These have been shown to result in a number of different crystal symmetries which arise due to tilting of the BO_6 octahedra about the crystallographic axes which have been rigorously analyzed in terms of group–subgroup

*Corresponding author. Department of Chemistry, McMaster University, 1280 Main Street W., Hamilton, Ont., Canada L8S 4M1.
Fax: +1 905 521 2773.
E-mail address: lozano@mcmaster.ca (A.D. Lozano-Gorrín).

0022-4596/$ - see front matter © 2007 Elsevier Inc. All rights reserved.
doi:10.1016/j.jssc.2007.01.019

relationships both for random *B*-site occupation and *B*-site ordering [9–11].

Also, the compounds that belong to this family have a wide variety of interesting magnetic properties. If the cations *B* and Ru^{5+} are site ordered, long-range magnetic order is usually observed at low temperatures in spite of the fact that the Ru^{5+} sublattice is face centered cubic which is a geometrically frustrated lattice [12]. For example, both Sr_2ErRuO_6 and Sr_2YRuO_6 show *B*-site ordering and each orders antiferromagnetically at ~40 K [4] and ~26 K, respectively [1]. Unusual magnetic properties are observed when *B* and Ru^{5+} are random. Despite having a high concentration of magnetic cations on a non-frustrated (with a random distribution, the sublattice of the octahedral sites is primitive cubic) lattice, $BaLaNiRuO_6$ and Sr_2FeRuO_6 do not transform to a magnetically ordered state, but they do show a spin-glass transition [3]. This surprising behavior has been explained in terms of the frustration caused by competing superexchange interactions among the random distribution of Ni/Ru and Fe/Ru cations. Similar properties have been observed in a series of compounds $Sr_nLaCuRuO_{n+5}$ ($n = 1,2,3$) and Sr_nFeRuO_{n+4} ($n = 3, 4$) [5,6].

In this paper, we investigate the potential solid solution between $SrRuO_3$ and $SrCoO_3$. Apart from the end members, only Sr_2CoRuO_6 has been reported [7]. In general, one expects random occupation of the *B*-site due to the small size differences between Ru^{4+}/Ru^{5+} and Co^{3+}/Co^{4+} in either spin state. $SrRuO_3$ shows the *Pnma* structure and $SrCoO_3$ is cubic, *Pm*3*m* [13,14]. Of course stoichiometric $SrCoO_3$ cannot be prepared under ambient oxygen pressure such as used here and a more likely composition under these conditions is $SrCoO_{2.64}$ which is also cubic, *Pm*3*m* [15]. Sr_2CoRuO_6 crystallizes in *I*2/*c* with random *B*-site occupation [7]. Both $SrRuO_3$ and $SrCoO_3$ are metallic ferromagnets with $T_c = 155$ and 320 K, respectively, so the magnetic properties are explained by the itinerant electron model, while Sr_2CoRuO_6 is reported to show spin-glassy behavior [7,14,16–19]. Here we investigate several members of the potential solid solution, $Sr_2Ru_{2-x}Co_xO_{6-y}$ using X-ray diffraction and SQUID magnetometry. The issue of the oxidation and spin states of Co is addressed using high-resolution electron energy loss spectroscopy (EELS).

2. Experimental

$Sr_2Ru_{2-x}Co_xO_6$ ($0.5 \leqslant x \leqslant 1.5$) samples were prepared by solid-state reactions from stoichiometric amounts of Ru (99.9%), $Co(Ac)_2 \cdot 4H_2O$ (99%) and $SrCO_3$ (>98%). The mixtures were heated in air overnight for carbonate decomposition at 850 °C and then for 5 days at 1050 °C with several intervening regrindings to obtain the oxides as polycrystalline materials. The samples were cooled in the furnace from the reaction temperature to room temperature.

2.1. X-ray diffraction

Powder X-ray diffraction at room temperature was carried out in a PANalytical X'Pert PRO diffractometer with X'Celerator detector and primary monochromator, using Cu$K\alpha_1$ radiation, in the angular range $10° < 2\theta < 120°$, by step scanning in equivalent increments of 0.02°. The data were analyzed using the Rietveld method [20] using the GSAS program [21] and its graphical user interface EXPGUI [22]. Both peak shape and background were described using a pseudo-Voigt function with 19 and 12 terms, respectively.

2.2. Thermal analysis

Thermogravimetric analysis was carried out in a reducing atmosphere by heating in an atmosphere of H_2 from room temperature to 780 °C. The samples were reduced to the elements (Ru and Co) and to the oxide SrO, permitting a determination of the original oxygen content, δ, in $Sr_2Ru_{2-x}Co_xO_{6-\delta}$.

2.3. Magnetic measurements

Magnetic susceptibility data were performed using a SQUID MPMS magnetometer from Quantum Design in the temperature range from 2 to 300 K and by using an oven in the range from 300 to 600 K. Measurements of susceptibility as a function of external magnetic field up to 1 kOe were performed. Susceptibility was measured using field-cooled (FC) and zero-field-cooled (ZFC) scans.

2.4. EELS measurements

EELS experiments have been carried out on a 200 keV transmission electron microscope (TEM) equipped with a monochromator and a high-resolution spectrometer, as described elsewhere [23]. This system enabled the acquisition of the Co-L_{23} edge in the three compounds $Sr_2Ru_{2-x}Co_xO_6$ with $x = 0.5$, 1.0 and 1.5 with an energy resolution of 0.2 eV (measured as the full-width at half-maximum (FWHM) of the zero loss peak) and a probe size of few tens of nanometers. In order to improve the energy resolution and keep a reasonable signal-to-noise ratio, several spectra have been recorded for each compound with relatively short acquisition time and summed. These spectra have been recorded in diffraction mode using a large collection angle (>10 mrad). The background has been fitted on the pre-edge region with a power law, extrapolated and subtracted to the edge using standard procedures to get the final spectra displayed hereafter. The TEM samples were prepared by crushing the powders in ethanol and dispersing the suspension on a holey carbon-covered Cu grid. Care has been taken to record the spectra on selected areas of the samples, thin enough to ensure a negligible contribution of the multiple inelastic scattering to the spectral shape.

3. Results and discussion

3.1. Structural characterization

X-ray powder diffraction patterns reveal that all the samples, except for $x = 0.67$, have been obtained as essentially pure phases. The presence of trace-impurity phases was observed in the form of very weak reflections identified as Co_3O_4 for $Sr_2Ru_{1.5}Co_{0.5}O_6$, Sr_2RuCoO_6 and $Sr_2Ru_{0.5}Co_{1.5}O_6$, and CoO for $Sr_2Ru_{1.33}Co_{0.67}O_6$ and $Sr_2Ru_{0.67}Co_{1.33}O_6$. In all of the compounds studied with Sr^{2+} on the *A*-site, the Goldschmidt tolerance factors imply a reduction of symmetry from cubic. The patterns for the various phases have been refined in different space groups using the group/subgroup relationships developed in Ref. [10] as a guide. In all cases, and because ruthenium and cobalt occupy the same site in the crystal, isotropic parameters for both atoms were refined using the same value. For the phases with the lowest ruthenium content, $Sr_2Ru_{0.5}Co_{1.5}O_6$ (Fig. 1) and $Sr_2Ru_{0.67}Co_{1.33}O_6$, the orthorhombic space group *Imma* (No. 74) gave the best result in comparison with other models based on *I*2/*c* or *I*4/*mcm* which are possible according to Ref. [10]. Sr_2RuCoO_6 (Fig. 2(a)) was refined in space group *I*2/*c* (No. 15) in agreement with Ref. [7]. A refinement was also done in *Pnma* giving a poorer overall fit, with $R_{wp} = 8.71\%$ and $\chi^2 = 2.68$, compared to corresponding values of 4.70% and 1.70 for *I*2/*c*. Fig. 2(b) shows the good fitting achieved using *I*2/*c* for a selected part of the profile, while Fig. 2(c) shows a worse fitting for *Pnma*. The data for $Sr_2Ru_{1.33}Co_{0.67}O_6$ (Fig. 3) could not be refined using a single phase but rather as a mixture of two phases, orthorhombic *Pnma* (No. 63) and monoclinic *I*2/*c*. The weight percentages were 37.80% for the *Pnma* and 62.20% for *I*2/*c*. Also, the refinement revealed that the Ru/Co ratio is different between the *Pnma* and *I*2/*c* phases with *B*-site contents of 91(1)% Ru/9(1)% Co for the former and 41(2)% Ru/59(2)% Co in the latter case. Thus the phase separation in this case is associated with segregation into an Ru-rich phase (*Pnma*) with a large cell volume and a Co-rich phase (*I*2/*c*) with a small cell volume. Finally, $Sr_2Ru_{1.5}Co_{0.5}O_6$ was refined in *Pnma* (No. 63). Cell parameter values and agreement factors obtained from the Rietveld refinement are shown in Table 1. As can be seen, the cell volume increases systematically with increasing Ru content.

Ru/Co–O distances for each phase are shown in Table 2. In order to interpret these results, it is necessary to consider the distribution of oxidation states and spin states for Ru and Co. For example, one expects to find both Ru^{4+}/Ru^{5+} and Co^{3+}/Co^{4+}. While there is little ambiguity concerning the spin state for the Ru species, both oxidation states for Co can exist in either high- or low-spin states which have very different radii. Also, it is important to determine the oxygen content in $Sr_2Ru_{2-x}Co_xO_{6-\delta}$. To these ends, the oxidation and spin states of Co were monitored using EELS and the oxygen content was determined using reductive thermogravimetric analysis.

3.2. Reductive thermogravimetry

The results of the hydrogen reductions according to the equation:

$$Sr_2Ru_{2-x}Co_xO_{6-\delta} + (4-\delta)H_2 \rightarrow 2SrO + (2-x)Ru + xCo + (4-\delta)H_2O \quad (1)$$

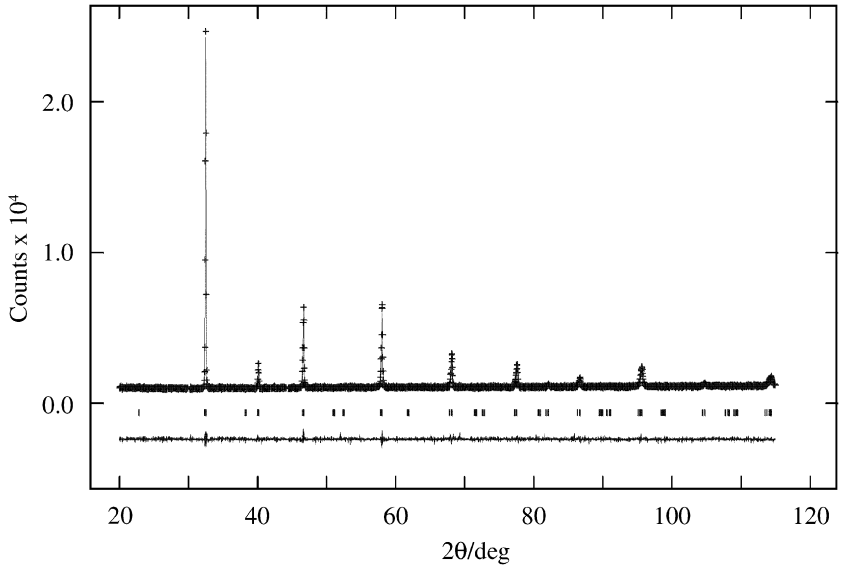

Fig. 1. Rietveld fitting of the X-ray diffraction pattern for $Sr_2Ru_{0.5}Co_{1.5}O_6$ in *Imma*. The data are the crosses, the solid line is the fitted profile, the vertical tic marks locate the Bragg peaks and the difference plot is shown at the bottom.

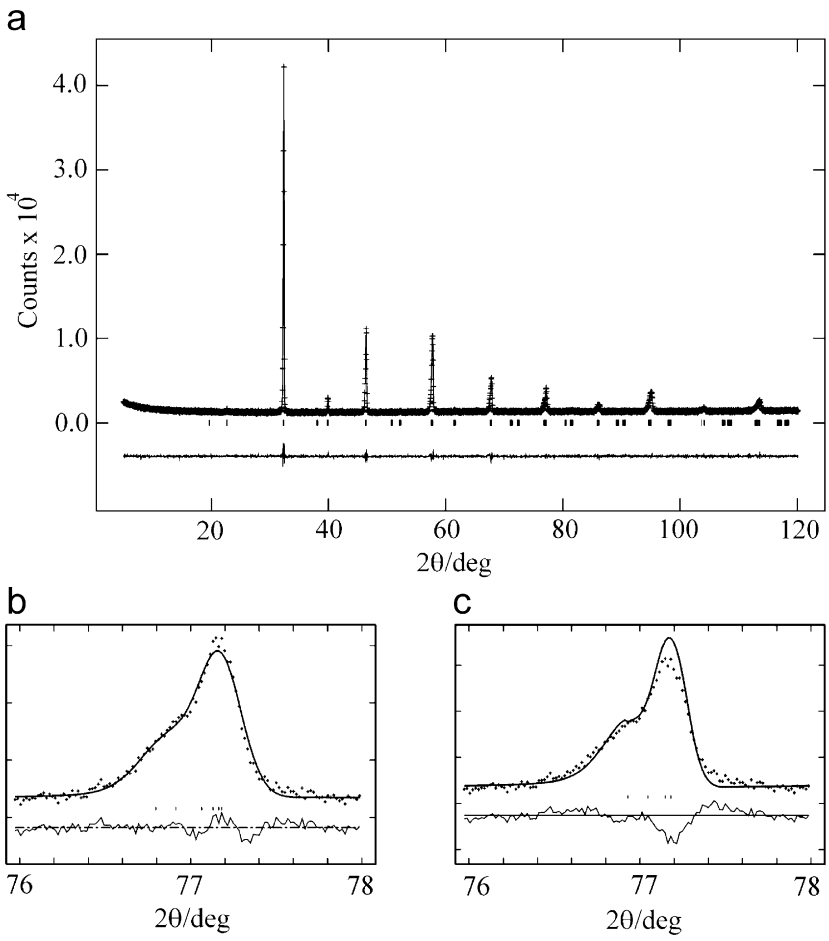

Fig. 2. Rietveld fitting of the X-ray diffraction pattern for $Sr_2Ru_{1.0}Co_{1.0}O_6$ in $I2/c$. The data are the crosses, the solid line is the fitted profile, the vertical tic marks locate the Bragg peaks and the difference plot is shown at the bottom (a). Comparison at about 77°2θ between fittings with $I2/c$ (b) and *Pnma* (c).

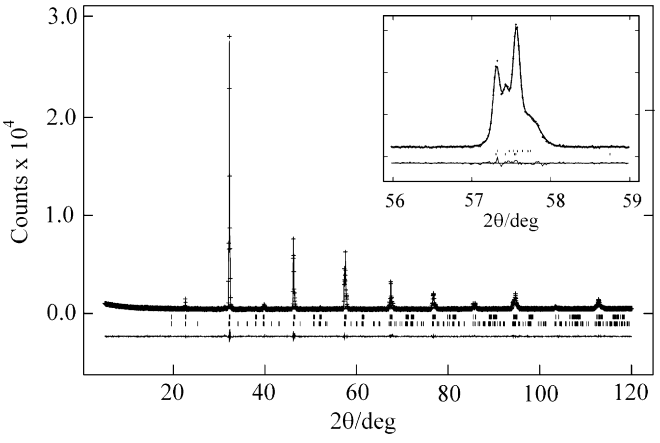

Fig. 3. Rietveld fitting of the X-ray diffraction pattern for $Sr_2Ru_{1.33}Co_{0.67}O_6$ as a two-phase sample in $I2/c$ and *Pnma*. The data are the crosses, the solid line is the fitted profile, the vertical tic marks locate the Bragg peaks and the difference plot is shown at the bottom. The inset highlights a part of the pattern demonstrating the presence of two phases.

for all compositions are collected in Table 3. It is clear that the oxygen non-stoichiometry is negligible even for those members rich in Co.

3.3. Energy loss near-edge fine structure measurements

In order to determine the formal valency and the spin state of Co atoms, electron energy loss measurements have been carried out on the Co-L_{23} edge. The L_{23} edge fine structure of transition metals observed in X-ray absorption or electron energy loss spectroscopies is a very sensitive probe of the valence [24,25], orbital [26] and spin state of the ion [27]. This edge corresponds to the excitation of a $2p$ core electron mainly to the unoccupied $3d$ states, i.e., to the transition from the $2p^6 3d^n$ ground state to the $2p^5 3d^{n+1}$ excited electronic configuration. The experimental Co-L_{23} spectra recorded in $Sr_2Ru_{1.5}Co_{0.5}O_6$, $Sr_2Ru_{1.0}Co_{1.0}O_6$ and $Sr_2Ru_{0.5}Co_{1.5}O_6$ are displayed in Fig. 4. As indicated in the figure, the large $2p$ core-hole spin–orbit coupling is responsible for the splitting of the edge in two main parts (the L_3 and L_2 edges), the spectral shape being mainly related to the multiplet structure of the final state. The L_3 edge is formed by a pre-eminent central peak occurring at about 781 eV with a shoulder visible on its low-energy side and a large tail on the high-energy side. The L_2 edge exhibits only two broad structures of low intensity at 795 and 796 eV. These features are very similar in the three

Table 1
Cell parameters and reliability factors obtained from the Rietveld refinement

Space group	Parameter a (Å)	Parameter b (Å)	Parameter c (Å)	Angle β (deg.)	V (Å^3)	R_p	R_{wp}	R_{exp}
$Sr_2Ru_{0.5}Co_{1.5}O_6$								
Imma	5.49844(4)	7.77894(9)	5.52670(4)	—	236.388(17)	2.81	3.58	2.93
$Sr_2Ru_{0.67}Co_{1.33}O_6$								
Imma	5.50981(10)	7.79237(14)	5.51974(13)	—	236.9870(30)	3.04	3.93	3.11
Sr_2RuCoO_6								
*I*2/*c*	5.52699(3)	5.52319(7)	7.84166(15)	90.1714(10)	239.379(7)	3.71	4.70	3.61
$Sr_2Ru_{1.33}Co_{0.67}^{O}$								
Pnma	5.53699(5)	5.57034(4)	7.83996(7)	—	241.8070(30)	3.98	5.18	4.12
*I*2/*c*	5.55973(11)	5.53533(8)	7.81109(14)	90.2644(12)	240.383(8)			
$Sr_2Ru_{1.5}Co_{0.5}O_6$								
Pnma	5.53745(4)	5.57190(3)	7.84260(5)	—	241.9770(20)	5.49	7.30	4.97

Table 2
Ru/Co–O distances

Space group	Maximum distance Ru/Co–O1	Minimum distance Ru/Co–O1	Maximum distance Ru/Co–O2	Minimum distance Ru/Co–O2	Averaged distance Ru/Co–O
$Sr_2Ru_{0.5}Co_{1.5}O_6$					
Imma	1.953(6)	—	1.94901(23)	—	1.951
$Sr_2Ru_{0.67}Co_{1.33}O_6$					
Imma	1.94945(8)	—	1.95011(5)	1.94837(5)	1.94931
Sr_2RuCoO_6					
*I*2/*c*	1.9671(9)	—	1.976(9)	1.958(7)	1.967
$Sr_2Ru_{1.33}Co_{0.67}O_6$					
Pnma	1.999(30)	1.941(31)	2.035(4)	—	1.992
*I*2/*c*	1.9574(5)	—	1.952(5)	1.997(5)	1.969
$Sr_2Ru_{1.5}Co_{0.5}O_6$					
Pnma	1.991(15)	1.987(15)	1.9950(21)	—	1.991

Table 3
Results of the reductive weight loss analysis for $Sr_2Ru_{2-x}Co_xO_{6-\delta}$

Compound	% wt. loss	δ [$\pm$0.05]
$Sr_2Ru_{1.50}Co_{.50}O_{6-\delta}$	14.37	−0.07
$Sr_2Ru_{1.33}Co_{.67}O_{6-\delta}$	14.20	0.06
$Sr_2Ru_{1.00}Co_{1.00}O_{6-\delta}$	15.24	−0.13
$Sr_2Ru_{0.67}Co_{1.33}O_{6-\delta}$	15.27	0.02
$Sr_2Ru_{0.50}Co_{1.50}O_{6-\delta}$	15.60	0.00

compounds and within our experimental resolution; no substantial modification of this edge can be detected. The low-intensity peak visible for $Sr_2Ru_{1.0}Co_{1.0}O_6$ at about 778–779 eV is thought to be due to the presence of Co_3O_4 impurities.

In order to determine the formal valency and the spin state of the Co atoms corresponding to these experimental signatures, ligand-field multiplet calculations have been performed [28]. The best agreement with the experimental spectra has been found for high-spin Co(III) in an octahedral field with $10Dq = 1.15$ eV and is displayed in Fig. 4. When directly compared to ionic calculations [29], the experimental spectra show a poor agreement with the theoretical predictions for Co(III). This is mainly due to the hybridization taking place between the transition metal and the ligand atoms in the solid state. These effects can be included using charge transfer multiplet calculations, where the interactions between the different low-lying configurations $3d^6$, $3d^7L$, $3d^8L^2$,… (where L stands for a ligand hole) are taken into account. However, a simple alternative to charge transfer calculations, especially in the absence of visible satellite structures on the experimental spectra, consists in the reduction of the Slater integrals [30] describing electron–electron Coulomb and exchange interactions. In our case, they have been reduced to 55% of their atomic values for *d–d* interactions, and to 70% for the *p–d* interactions. This difference in the reduction factors is justified by the fact that the 2*p* core states are not affected by the hybridization. The atomic values for the 3*d*

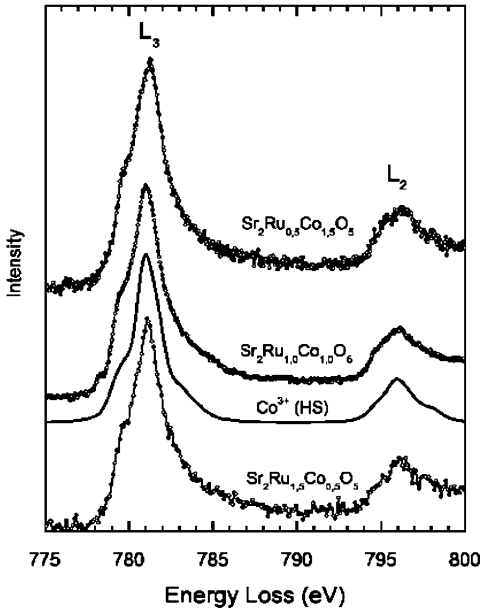

Fig. 4. Experimental Co-L_{23} edge (open circles) recorded in $Sr_2Ru_{2-x}Co_xO_5$ ($x = 0.5$, 1, 1.5) compared to ligand-field multiplet calculation for Co^{3+} in O_h symmetry (solid line).

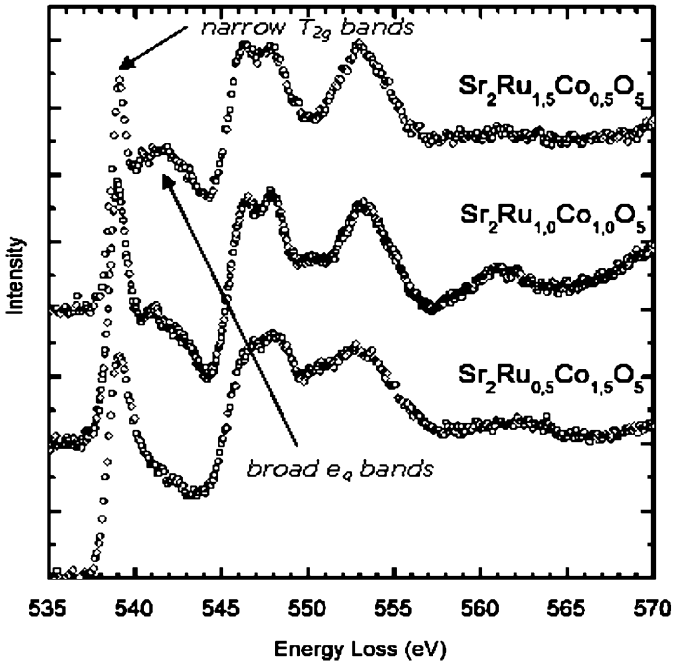

Fig. 5. Experimental O-K edge (open circles) recorded in $Sr_2Ru_{2-x}Co_xO_5$ ($x = 0.5$, 1, 1.5) showing clear sharp peaks corresponding to the T_{2g} bands and broad peaks corresponding to the e_g bands.

spin–orbit coupling have been used. Lorentzian broadenings of FWHM 0.3 and 0.43 eV [31] accounting for the core-hole finite lifetime have been applied to L_3 and L_2 edges, respectively. Finally, a Gaussian broadening of FWHM 0.2 eV has been applied to the spectrum to account for the instrumental resolution. Using these parameters, all the structures observed on the experimental spectra are reproduced, the overall good agreement between theoretical and experimental spectra thus indicates a high-spin Co(III). A comparison with other experimental signatures of Co(III) with an established spin state recorded in different compounds also confirms this result. Our experimental spectra are indeed comparable to high-spin Co(III) recorded in Sr_2CoO_3Cl [32] but clearly different from low-spin Co(III) recorded in $EuCoO_3$ [32], $LiCoO_2$ [33] or low-temperature $LaCoO_3$ [34]. However, if the presence of low-spin Co(III) can be safely excluded, the precise determination of the formal valency of Co is not straightforward in this case. The experimental L_{23} edge of high-spin Co(IV) recorded in stoichiometric $SrCoO_3$ [33] shows indeed strong similarities with the spectral shape of high-spin Co(III). Thus, a possible mixture of high-spin Co(III) and Co(IV) cannot be clearly ruled out from our experimental data.

Corroborating evidence for Co^{3+}(HS) can be found in the O *K*-edge data, Fig. 5. Note the presence of two low-energy features, a sharp peak which can be attributed to transitions to empty t_{2g} states and a broader peak attributed to transitions to empty e_g states [technically, transitions to O *p*-states strongly hybridized with Co/Ru t_{2g} and e_g states]. Note that the intensity ratio of the e_g/t_{2g} peaks decreases as the Co/Ru ratio in the materials increases. If Co^{3+} were in the LS state (t_{2g}^6), there would be no expected change in the e_g/t_{2g} intensity ratio as a function of increasing Co concentration whereas for the HS state ($t_{2g}^4e_g^2$) the observed effect can be understood qualitatively. Thus, the O *K*-edge data are also consistent with Co^{3+} in the HS state for all studied compositions.

3.4. Summary of the structure results

Given that the high-spin state has been established for Co^{3+} and Co^{4+} and that oxygen non-stoichiometry is ruled out, it is possible to propose a distribution of oxidation and spin states for both Ru and Co for all of the solid solution members. These proposals are displayed in Table 4 along with the observed and calculated Ru(Co)–O distances. The calculated distances are derived from the established ionic radii for the cations and a radius of 1.38 Å for O^{2-} [35]. The agreement is clearly acceptable. At this stage, it is desirable to summarize the findings of the structural refinements and to look for systematic behavior. An attempt to do this is shown in Fig. 5 in which the sequence of space groups and Glazer tilt systems is seen to develop systematically as a function of increasing Goldschmidt tolerance factor (Fig. 6):

$$Pnma(a^+b^-b^-) \rightarrow I2/c(a^-b^-b^-) \rightarrow Imma(a^0b^-b^-) \rightarrow Pm3m(a^0a^0a^0).$$

That is, there is a smooth passage from three-tilt to two-tilt to zero-tilt structures with increasing tolerance factor. A fifth structure could be expected, the single-tilt ($a^0a^0c^-$) *I*4/*mcm*, between the *Imma* and *Pm*3*m* phases, but it was not detected in the composition range studied. The

Table 4
Comparison of observed and calculated Ru(Co)–O distances for proposed distribution of Ru and Co oxidation and spin states in $Sr_2Ru_{2-x}Co_xO_6$

x	Co^{3+}(HS)	Co^{4+}(HS)	Ru^{4+}	Ru^{5+}	$\langle Ru(Co)–O\rangle_{obs}$ (Å)	$\langle Ru(Co)–O\rangle_{calc}$ (Å)
0.20	0.20	0.0	1.6	0.2	1.99	1.99
0.50	0.50	0.0	1.0	0.5	1.99	1.99
1.0	1.0	0.0	0.0	1.0	1.97	1.97
1.18	0.82	0.36	0.0	0.82	1.97	1.96
1.33	0.65	0.68	0.0	0.67	1.95	1.95
1.50	0.50	1.0	0.0	0.50	1.95	1.94

Note that the entries for $x = 0.20$ and 1.18 derive from the phase-separated $x = 0.67$ material.
Revised effective ionic radii (Å) by R.D. Shannon [35]: Co^{3+}(HS) = 0.61, Co^{4+}(HS) = 0.53, Ru^{4+} = 0.62, Ru^{5+} = 0.565, O^{2-} = 1.38.

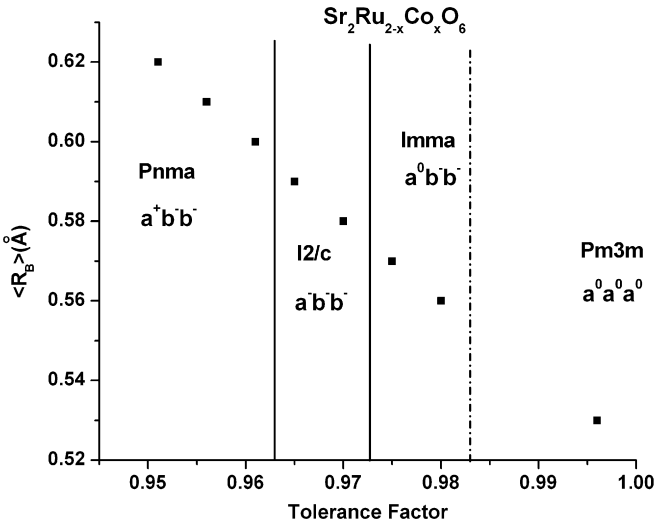

Fig. 6. Correlation between the average *B*-site radius, the Goldschmidt tolerance factor and the sequence of space groups and Glazer tilt systems found for the perovskite solid solution $Sr_2Ru_{2-x}Co_xO_6$.

tolerance factor, t, is defined for an ABO_3 perovskite as

$$t = (R_A + R_O)/\sqrt{2}(R_B + R_O)$$

and the radii, R_A, R_B and R_O, are taken from [35] (also see footnote in Table 2).

3.5. Magnetic properties

Magnetic susceptibility at lower temperatures shows a strong irreversibility of the ZFC and FC curves below 150–160 K and prominent maxima in the ZFC data. Fig. 7 shows magnetic susceptibility behavior as a function of temperature for $Sr_2Ru_{0.5}Co_{1.5}O_6$, Sr_2RuCoO_6 and $Sr_2Ru_{1.5}Co_{0.5}O_6$, and the magnetic susceptibility data at 300–600 K which obeys the Curie–Weiss law. For all phases in this solid solution, one sees an inflection around 150–160 K in the ZFC data. This is assigned to residual traces of ferromagnetic $SrRuO_3$ which was not observed in the X-ray diffraction data. For most of the cases, the ZFC/FC divergence starts at higher temperatures than the maximum, as has been observed for the compound

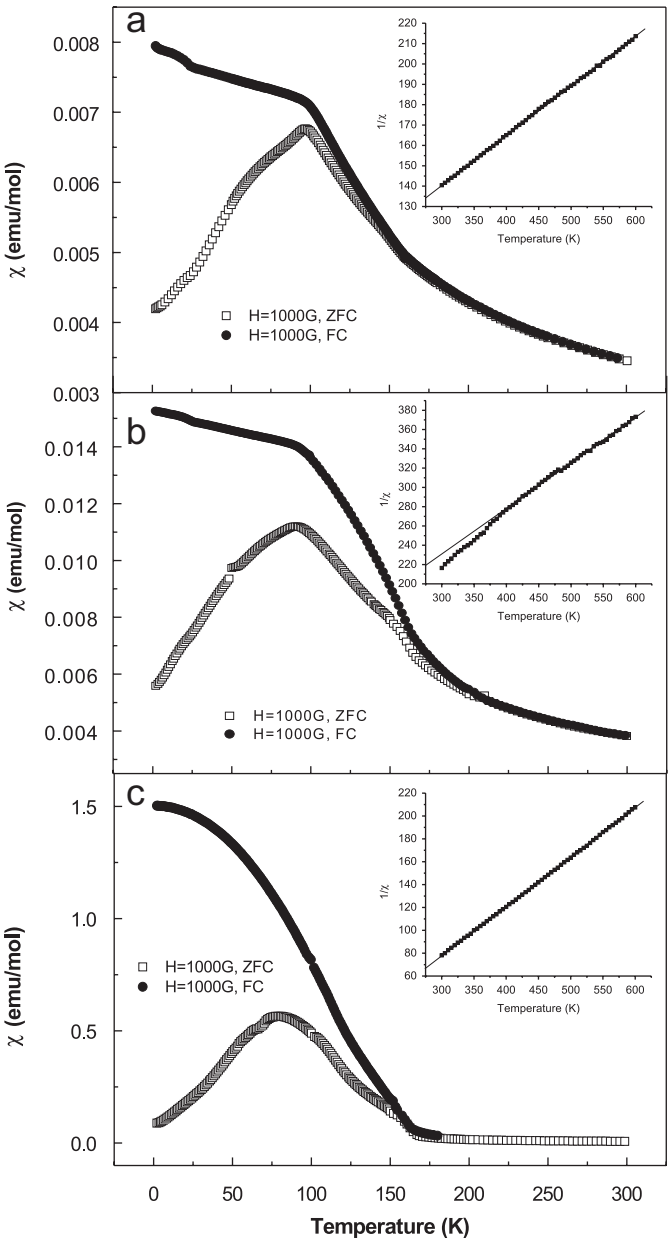

Fig. 7. Magnetic susceptibility for $Sr_2Ru_{0.5}Co_{1.5}O_6$ (a), Sr_2RuCoO_6 (b) and $Sr_2Ru_{1.5}Co_{0.5}O_6$ (c). The insets correspond to the data of the magnetic susceptibility at high temperature (300–600 K).

Table 5
Curie–Weiss fitting parameters for $Sr_2Ru_{2-x}Co_xO_6$

Compound	$C_{observed}$	θ (K)	T (χ_{max})[a]	$C^{s.o}_{total}$
$Sr_2Ru_{0.5}Co_{1.5}O_{5.5}$	4.12	−279.78	97	6.83
$Sr_2Ru_{0.67}Co_{1.33}O_{5.5}$	4.20	−270.15	92	6.19
Sr_2RuCoO_6	2.14	−198.14	90	4.90
$Sr_2Ru_{1.5}Co_{0.5}O_6$	2.32	119.11	78	2.87

Notes: $C^{s.o}_{total}$ for all compounds was calculated considering Ru^{5+}, Ru^{4+}, Co^{3+}(HS) and Co^{4+}(HS) according to Table 4.
[a]Temperature (K) of maximum susceptibility ZFC.

$CaRu_{1-x}Cu_xO_3$ [36]. The position of the maximum increases with increasing Co content from 78 K for $x = 0.5$ to 90 K for $x = 1.0$ to 97 K for $x = 1.5$. The value for $x = 1.0$ is in good agreement with that reported by Battle et al. [7] The maxima are broad in general and not typical of antiferromagnetic long-range order but rather of spin freezing. This conclusion needs confirmation by neutron diffraction or heat capacity.

Table 5 displays results of attempts to fit the higher-temperature data to the Curie–Weiss law. The calculated spin- only Curie constant, $C^{s.o.}$, was computed taking into account the oxidation and spin states of Table 4. In all cases, except for the most Ru-rich phase, $x = 0.5$, C^{obs} lies far below $C^{s.o.}$. This discrepancy is not necessarily unexpected. For example, spin-only values are not often realized in practice. Reported effective moments for cases where Co^{3+}(HS) is well documented, such as in the $BaLnCo_2O_5$ phases, lie in the range 3.1–4.5 μ_B [37,38]. The range of corresponding Curie constants ($C = \mu^2_{eff}/8$) is thus 1.20–2.53 emu K/mol, much reduced from the spin-only value of 3.0 emu K/mol. Also, one could expect a reduction of μ_{eff} for Ru^{4+} and Ru^{5+} due to spin–orbit coupling. Finally, the actual spin state of Co^{4+} ($3d^5$) is not clear. The Co $L_{2,3}$ EELS spectra of Co^{3+}(HS) and of $SrCoO_3$ where Co^{4+} is formally present are very similar as mentioned earlier but the spin state of the nominal Co^{4+} is not specified. So, while the Curie–Weiss law appears to hold at high temperatures for all of the compositions studied, the extracted Curie constants cannot be understood in a straightforward manner in terms of the oxidation and spin states of the species present. Nonetheless, the Weiss temperatures, θ_c, show a clear trend from negative for the Co-rich compositions to positive for the Ru-rich phases. Both $SrRuO_3$ and $SrCoO_3$ are itinerant electron ferromagnets, but the intermediate compositions all show spin-glass-like behavior and are likely to be semiconductors such as the intermediate phase Sr_2RuCoO_6 already studied by Battle et al. [7]. For these materials a localized electron model is more appropriate and the Goodenough–Kanamori rules can be applied [39]. Accordingly, assuming the correlations for 180° cation–anion–cation interactions, one expects the following: moderate ferromagnetic for $Co^{3+/4+}$(HS)–$Ru^{5+/4+}$ combinations, weak antiferromagnetic for $Ru^{5+/4+}$–$Ru^{3+/4+}$, but strong antiferromagnetic for $Co^{3+/4+}$–$Co^{3+/4+}$, both HS. Given the random distribution of *B*-site cations, clearly there is competition between ferro- and antiferromagnetic exchange within the solid solution which is consistent with the observed spin freezing transitions. Also, within the framework of this scenario, the positive θ_c value for the phases more rich in Ru is plausible, while the strongly negative θ_c for the most Co-rich phases can be understood.

4. Summary and conclusions

The perovskite solid solution $Sr_2Ru_{2-x}Co_xO_{6-\delta}$, $0.5 < x < 1.5$, has been studied by X-ray diffraction, thermogravimetry and d.c. magnetic susceptibility. The degree of oxygen non-stoichiometry was found to be negligible, i.e., δ–0 in all cases. The sequence of structures *Pnma–I2/c–Imma–Pm3m* was observed with increasing x (and increasing tolerance factor). In all cases, the Ru and Co ions were randomly distributed on the *B*-site. A miscibility gap was observed at $x = 0.67$ resulting in separation into Ru-rich *Pnma* and Co-rich *I2/c* phases. EELS studies of the Co L_3/L_2 and O *K*-edges established the presence of Co^{3+} in the high-spin state and ruled out the low-spin state for all compositions. The presence of Co^{4+} is compatible with the *L*-edge spectra. The observed Ru(Co)–O distances are consistent with a proposed distribution of Ru^{4+}, Ru^{5+}, Co^{3+}(HS) and Co^{4+}(HS) on the *B*-site for each studied composition. For phases rich in Co a large concentration of Co^{4+} is required to explain the observed distances. Magnetically, the materials display spin freezing behavior below ~100 K which is consistent with the *B*-site randomness and competing ferro- and antiferromagnetic exchange.

Acknowledgments

We are grateful to Dr. S. Lazar (Technical University Delft) for the help in the acquisition of the Electron Energy Loss Spectra and Prof. H.W. Zandbergen (Technical University Delft) for access to the monochromated TEM facilities of the National Centre for High Resolution Electron Microscopy, Delft. Funding from the NWO (The Netherlands) is acknowledged by G.A. Botton. J.E. Greedan and G.A. Botton thank the Natural Sciences and Engineering Research Council of Canada for support in the form of Discovery Grants. A.D. Lozano-Gorrín thanks the Spanish MEC for a postdoctoral fellowship and Frank Gibbs for thermogravimetric measurements at McMaster University.

References

[1] P.D. Battle, W.J. Macklin, J. Solid State Chem. 52 (1984) 138.
[2] I. Fernandez, R. Greatrex, N.N. Greenwood, J. Solid State Chem. 32 (1980) 97.
[3] P.D. Battle, T.C. Gibb, C.W. Jones, F. Studer, J. Solid State Chem. 78 (1989) 281.

[4] P.D. Battle, C.W. Jones, F. Studer, J. Solid State Chem. 90 (1991) 302.
[5] S.H. Kim, P.D. Battle, J. Magn. Magn. Mater. 123 (1993) 273.
[6] P.D. Battle, S.K. Bollen, A.V. Powell, J. Solid State Chem. 99 (1992) 267.
[7] S.H. Kim, P.D. Battle, J. Solid State Chem. 114 (1995) 174.
[8] M.T. Anderson, K.B. Greenwood, G.A. Taylor, K.R. Poeppelmeier, Prog. Solid State Chem. 22 (1993) 197.
[9] A.M. Glazer, Acta Crystallogr. B 28 (1972) 3384.
[10] P.M. Woodward, Acta Crystallogr. B 53 (1997) 32.
[11] C.J. Howard, B.J. Kennedy, P.M. Woodward, Acta Crystallogr. B 59 (2003) 463.
[12] J.E. Greedan, J. Mater. Chem. 11 (2001) 37.
[13] C.W. Jones, P.D. Battle, P. Lightfoot, W.T.A. Harrison, Acta Crystallogr. C 45 (1989) 365.
[14] I.S. Shaplygin, V.B. Lazerev, Russ. J. Inorg. Chem. 30 (1985) 3214; P. Bezdicka, A. Wattiaux, J.C. Grenier, M. Pouchard, P. Hagenmuller, Z. Anorg. Allgem. Chem. 619 (1993) 7.
[15] A. Nakatsuka, A. Yoshiasi, N. Nakayama, T. Mizota, H. Takei, Acta Crystallogr. C 60 (2004) i59.
[16] H. Taguchi, H. Shimada, H. Koizumi, Mater. Res. Bull. 15 (1980) 165.
[17] H. Taguchi, H. Shimada, H. Koizumi, J. Solid State Chem. 29 (1979) 221.
[18] P.B. Allen, H. Berger, O. Chauvet, L. Forro, T. Jarlborg, A. Junod, B. Reavz, G. Santi, Phys. Rev. B 53 (1996) 4393.
[19] A. Callghan, C.W. Moeller, R. Ward, Inorg. Chem. 5 (1966) 1572; J.M. Longo, P.M. Raccah, J.B. Goodenough, J. Appl. Phys. 39 (1968) 1327.
[20] H.M. Rietveld, J. Appl. Crystallogr. 2 (1969) 65.
[21] A.C. Larson, R.B. Von Dreele, General Structure Analysis System (GSAS), Los Alamos National Laboratory Report LAUR 86-748, 1994.
[22] B.H. Toby, J. Appl. Crystallogr. 34 (2001) 210.
[23] S. Lazar, G.A. Botton, F.T. Tichelaar, M.-Y. Wu, H.W. Zandbergen, Ultramicroscopy 96 (2003) 535.
[24] M. Abbate, F.M.F. de Groot, J.C. Fuggle, A. Fujimori, Y. Tokura, Y. Fujishima, O. Strebel, M. Domke, G. Kaindl, J. van Elp, B.T. Thole, G.A. Sawatsky, M. Sacchi, Phys. Rev. B 44 (1991) 5419.
[25] A.S. Sefat, G. Amov, M.-Y. Wu, G.A. Botton, J.E. Greedan, J. Solid State Chem. 178 (2005) 1008.
[26] J.-H. Park, L.H. Tjeng, A. Tanaka, J.W. Allen, C.T. Chen, P. Metcalf, J.M. Honig, F.M.F. de Groot, G.A. Sawatzky, Phys. Rev. B 61 (2000) 11506.
[27] G. van der Laan, B.T. Thole, G.A. Sawatsky, M. Verdaguer, Phys. Rev. B 37 (1988) 6587.
[28] F. de Groot, Coord. Chem. Rev. 249 (2005) 31.
[29] G. van der Laan, I.W. Kirkman, J. Phys.: Condens. Matter 4 (1992) 4189.
[30] F.M.F. de Groot, J. Electron Spectrosc. Relat. Phenom. 67 (1994) 74.
[31] J.C. Fuggle, J.E. Inglesfield (Eds.), Unoccupied electronic states, fundamentals for XANES, EELS, IPS and BIS, Topics in Applied Physics, vol. 69, Springer, Berlin.
[32] Z. Hu, H. Wu, M.W. Haverkort, H.H. Hsieh, H.-J. Lin, T. Lorentz, J. Baier, A. Reichl, I. Bonn, C. Felser, A. Tanaka, C.T. Chen, L.H. Tjeng, Phys. Rev. Lett. 92 (2004) 207402.
[33] F.M.F. de Groot, M. Abbate, J. van Elp, G.A. Sawatzky, Y.J. Ma, C.T. Chen, F. Sette, J. Phys.: Condens. Matter 5 (1993) 2277.
[34] M. Abbate, J.C. Fuggle, A. Fujimori, L.H. Tjeng, C.T. Chen, R. Potze, G.A. Sawatsky, H. Eisakia, S. Uchida, Phys. Rev. B 47 (1993) 16124.
[35] R.D. Shannon, Acta Crystallogr. A 32 (1976) 751.
[36] I.M. Bradaric, I. Felner, M. Gospodinov, Phys. Rev. B 65 (2001) 024421.
[37] A. Maignan, C. Martin, D. Pelloquin, N. Nguyen, B. Raveau, J. Solid State Chem. 142 (1999) 247.
[38] Y. Moritomo, T. Akimoto, M. Takeo, A. Machida, E. Nishibori, M. Takata, M. Sakata, K. Ohoyama, A. Nakamura, Phys. Rev. B 61 (2000) R13325.
[39] J.B. Goodenough, Magnetism and the Chemical Bond, vol. 179, Wiley, New York, 1966.